Arch. Metall. Mater. **71** (2026), 1, 293-299

DOI: https://doi.org/10.24425/amm.2026.157791

CHANGGYUN KIM[1], DO CUONG TUNG[1], HO LEE[2], INJOON SON[1*]

SELECTIVE Ni ELECTROLESS DEPOSITION ON FEMTOSECOND LASER-PATTERNED POLYTETRAFLUOROETHYLENE-COATED ANODIZED AA7075

Aluminum heat sinks are widely used in semiconductor and electrical applications because anodizing enhances both chemical stability and thermal performance. However, their rigid form can lead to adhesion failures and limits their integration into flexible or miniaturized devices. To address these challenges, this work presents a conceptual demonstration of integrating electrodes directly onto an anodized aluminum heat sink via surface patterning. First, AA7075 substrates were anodized under varying voltages (3 V and 8 V) and process schemes (one-step vs. two-step) to identify conditions that optimize pore formation. Next, a hydrophobic PTFE polymer layer was spin-coated onto the two-step, 8 V-anodized surface, achieving a contact angle exceeding 100°. Selective femtosecond laser patterning was then used to locally restore hydrophilicity, and electroless Ni plating from an MPN 5A bath enabled precise Ni electrode patterning on the anodized aluminum. Finally, plating time optimization (5 min vs. 10 min) demonstrated that a 5 min deposition produces the most well-defined electrode features. These results demonstrate the feasibility of selective electroless plating on anodized AA7075 surfaces.

Keywords: AA7075 aluminum; anodizing; Electroless Nickel plating; polytetrafluoroethylene (PTFE)

1. Introduction

Heat sink materials are essential for effectively managing the heat generated by electronic devices. Aluminum is an excellent heat-dissipation material because of its relatively high thermal conductivity. Among aluminum alloy series, AA7075 (Al – 5.6 wt.% Zn, 2.5 wt.% Mg, 1.6 wt.% Cu) is well known for its thermal conductivity of ~130 W m^{-1} K^{-1}, which is higher than that of typical 1xxx or 6xxx series alloys, making it suitable as a heat-sink material. The Zn and Mg contents promote uniform pore formation and mechanical robustness in the anodic oxide, while Cu improves adhesion of the oxide layer to the aluminum substrate. To improve chemical stability, aluminum is commonly anodized to form a robust Al_2O_3 barrier layer that protects against oxidation and wear [1]. However, conventional heat sinks remain rigid and require separate bonding of electrodes or sensors, which can introduce interfacial thermal resistance and adhesion issues in flexible or miniaturized devices [2]. Forming electrodes and components directly on an anodized aluminum substrate can address these limitations. Electrode formation on a substrate is typically achieved through patterning techniques, and various studies have explored electrode patterning. For example, Yang et al. deposited electrode patterns using screen printing, [3] but screen printing has limitations in resolution and coverage, making it difficult to apply to anodic oxide films. Additionally, Kim et al. utilized photolithography to pattern SnO_2, achieving interfacial stability, [4] but photolithography requires multiple time-consuming steps, including masking and wet etching. More recently, Jha et al. demonstrated electroless Ni patterning by directing a laser beam onto palladium acetate sealed within anodized layers [5]. In this study, we present a conceptual demonstration of direct electrode integration on anodized aluminum through surface-energy–driven patterning. First, a thin PTFE layer is applied to render the entire Al_2O_3 surface hydrophobic. A focused laser then selectively ablates the PTFE, locally restoring hydrophilicity in the patterned regions. Finally, solution-based electroless Ni plating deposits conductive traces only within the laser-activated motifs. This mask-free approach eliminates complex lithography or transfer processes and enables low-profile, conformal electrode networks directly on anodized heat sinks for flexible electronics and microelectromechanical systems (MEMS) applications.

[1] KYUNGPOOK NATIONAL UNIVERSITY, SCHOOL OF MATERIALS SCIENCE AND ENGINEERING, DEPARTMENT OF MATERIALS SCIENCE AND METALLURGICAL ENGINEERING, KOREA
[2] KYUNGPOOK NATIONAL UNIVERSITY, SCHOOL OF MECHANICAL ENGINEERING, KOREA
* Corresponding author:ijson@knu.ac.kr

2. Experimental

2.1. Sample fabrication

A 25 mm × 25 mm AA7075 plate was used as the substrate. The substrate was first degreased by alkaline cleaning for 30 s and then immersed in 1-M KOH solution for the same duration. Subsequently, anodizing of the AA7075 plate was carried out in sulfuric acid solutions of different concentrations (10, 20, and 30 wt.%) under various applied voltages (3, 8, and 13 V). For additional two-step anodizing, the samples were immersed in 1 M KOH for 10 min and then in 20 wt% HNO_3 for 5 min after the first anodizing step, followed by re-anodizing in a sulfuric acid solution. Afterward, a PTFE solution was spin-coated onto the anodized AA7075 surface and the coated samples were heat-treated at 150°C for 30 min. Laser patterning was conducted using a femtosecond Yb:YAG laser with a pulse duration of 350 fs. Finally, electroless nickel plating was performed on the laser-patterned areas using a commercial medium-phosphorus electroless Ni solution (MPN 5A, KPM Tech, Korea; ≈5 wt.% P) at pH 4.5-4.7 and 80°C with magnetic stirring at 300 rpm for 5-10 min.

2.2. Sample analysis

The surfaces of AA7075 after one-step and two-step anodizing were analyzed using field-emission scanning electron microscopy (FE-SEM, JSM-IT700HR, JEOL, Japan). Surface morphologies of the aluminum and coating layers were obtained using a secondary electron detector at an accelerating voltage of 15 kV. Elemental maps of Al and Ni after Ni deposition were also acquired using an Oxford Instruments EDS detector. Changes in pore density after the additional anodizing step were evaluated, and pore density was quantified using ImageJ software. The surface hydrophobicity of the PTFE-coated and anodized samples was measured using a contact angle analyzer (Phoenix 300, Korea) with a drop volume of 1 μL and the instrument's built-in analysis software. The presence of the PTFE coating on the anodized AA7075 surface was confirmed by energy-dispersive X-ray spectroscopy (EDS) and Fourier-transform infrared spectroscopy (FT-IR, Nicolet iS20, Thermo Scientific, USA). ATR-FTIR spectra (3200-400 cm^{-1}) were acquired using a Smart iTR™ single-reflection diamond ATR accessory (1.5 mm crystal, 42° incidence, ~2 μm penetration depth) by pressing each Al sample (~1 N) onto the crystal with the integrated pressure arm.

3. Results and discussion

3.1. Surface Morphology of anodized AA7075

Fig. 1 illustrates the sample fabrication process for selective electroless Ni deposition on PTFE-coated AA7075 that was patterned using a femtosecond laser. After degreasing, pores were formed on the surface when AA7075 was anodized in a sulfuric acid solution. Compared with other electrolytes (CrO_3, $H_2C_2O_4$, and H_3PO_4), sulfuric acid produced a more uniform pore structure.[6] Subsequently, a hydrophobic surface was created by spin-coating PTFE onto the anodized surface. Selected areas were then exposed to a femtosecond laser, which is known to be well suited for precise patterning without generating a heat-affected zone [7]. Anodizing AA7075 also offers the advantage of increasing the surface area. To investigate the effect of anodizing conditions, anodizing was performed under different voltages (3, 8, and 13 V) and sulfuric acid concentrations (10, 20, and 30 wt.%). The resulting surfaces of anodized AA7075 are shown in Fig. 2. The images in the leftmost column correspond to AA7075 anodized in 10 wt.% H_2SO_4, exhibiting a dark-blue appearance, whereas samples treated at higher acid concentrations displayed progressively grayish surfaces. Figs. 2a, 2d, and 2g show the dimples and pores formed on the anodized surface, and a higher sulfuric acid concentration resulted in a greater number of dimples and pores. Similar increases in pore density with increasing sulfuric acid concentration were reported by Pei et al. [8]. In addition, higher anodizing voltages led to the formation of more pores on the anodized AA7075 surface. However, when AA7075 was anodized at 13 V in a 30 wt.% sulfuric acid solution, burning occurred and cracks developed

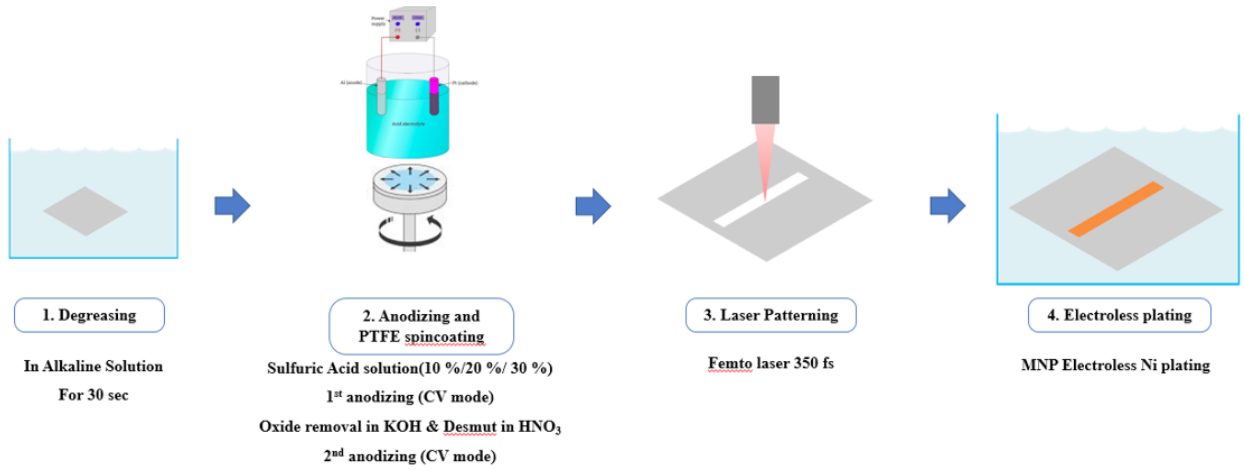

Fig. 1. Process for selective electroless nickel plating after femtosecond laser patterning on PTFE-coated AA7075

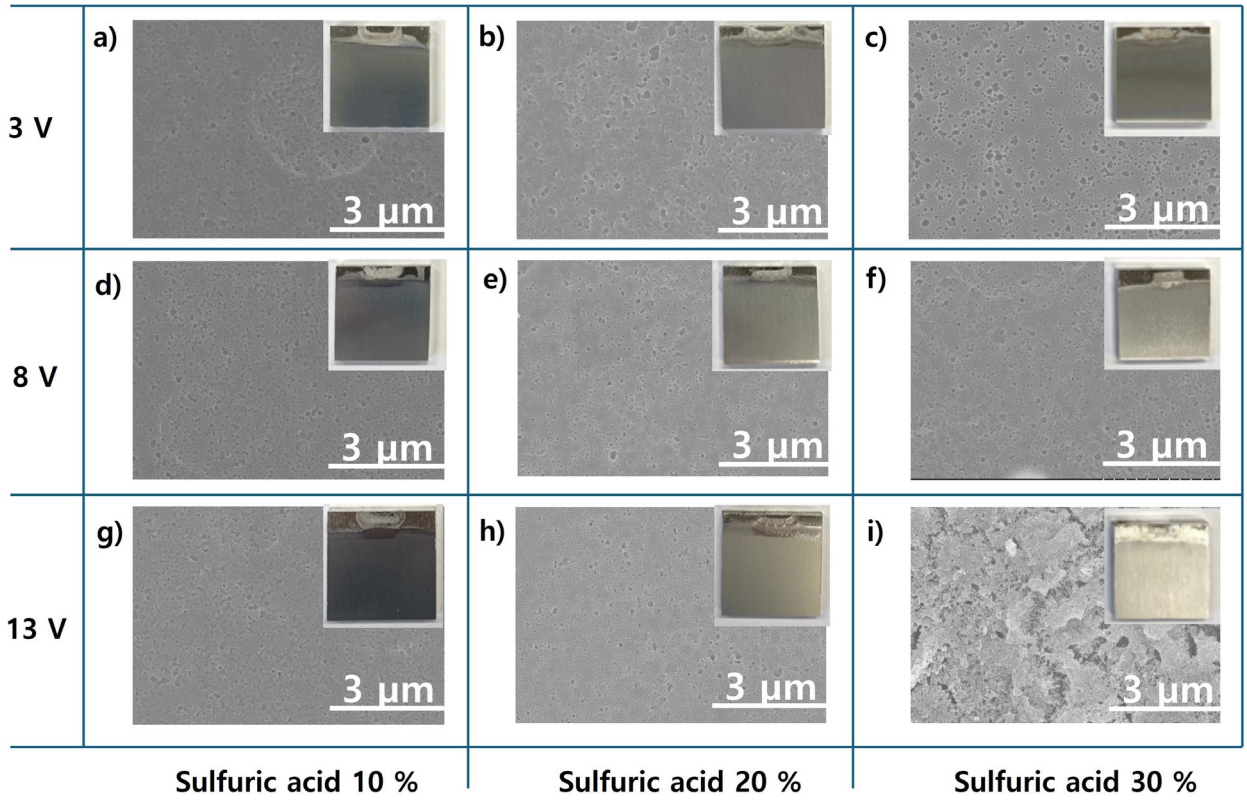

Fig. 2. SEM images of aluminum samples anodized at different voltages. a), b), c) Surfaces of samples anodized at 3 V in sulfuric acid solutions with concentrations of 10%, 20%, and 30%, respectively; d), e), f) Surfaces of samples anodized at 8 V in sulfuric acid solutions with concentrations of 10%, 20%, and 30%, respectively; g), h), i) Surfaces of samples anodized at 13 V in sulfuric acid solutions with concentrations of 10%, 20%, and 30%, respectively

across the surface. Chung et al. reported similar crack formation caused by severe anodizing reactions in high-concentration sulfuric acid solutions [9].

Increasing the regularity of pores can lead to more efficient heat dissipation. Furthermore, Gonzalez et al. reported that ordered anodizing can improve corrosion resistance [10]. To enhance pore regularity, a two-step anodizing process with an additional oxide-removal step was employed. Masuda et al. previously demonstrated that forming a concave "seed" layer and removing the anodic oxide after the first anodizing step results in more regular pore ordering during the second anodizing step [11]. Based on this concept, we compared the surface morphologies obtained from one-step and two-step anodizing of AA7075 (Fig. 3).

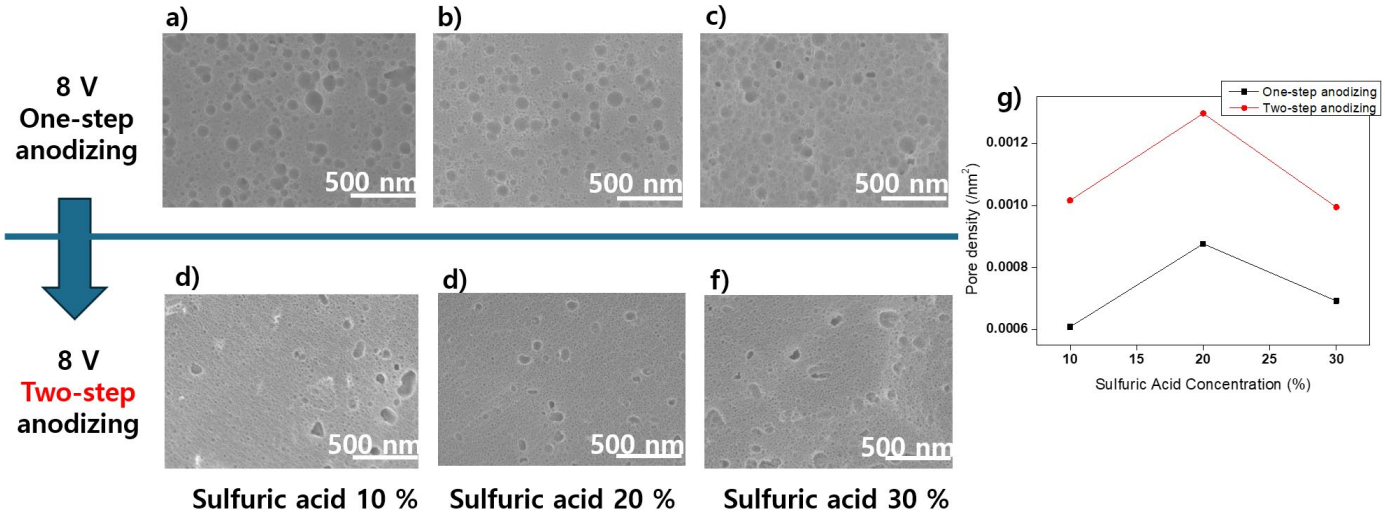

Fig. 3. Surface morphology of one-step VS two-step anodized AA7075. a) Sample anodized at 8 V in a 10% sulfuric acid solution (one-step anodizing); b) Sample anodized at 8 V in a 20% sulfuric acid solution (one-step anodizing); c) Sample anodized at 8 V in a 30% sulfuric acid solution (one-step anodizing); d) Sample anodized at 8 V in a 10% sulfuric acid solution (two-step anodizing); e) Sample anodized at 8 V in a 20% sulfuric acid solution (two-step anodizing); f) Sample anodized at 8 V in a 30% sulfuric acid solution (two-step anodizing)

After one-step anodizing, an irregular surface containing large dimples and small pores was observed (Figs. 3a-3c). The formation of large dimples may be attributed to the interconnection or coalescence of adjacent pores [12]. In contrast, the surfaces of the two-step anodized samples showed fewer dimples than those anodized in a single step. In addition to the improved pore regularity, the two-step anodized AA7075 samples exhibited a higher pore density when anodized at 8 V within the sulfuric acid concentration range of 10-30 wt.%.

3.2. Hydrophobicity of PTFE-Coated Anodized AA7075

TFE was selected as the hydrophobic coating material for anodized AA7075. Ruan et al. confirmed the mechanical stability and hydrophobicity of PTFE films [13]. The PTFE film was deposited onto the anodized AA7075 surface by spin coating and subsequently heat-treated on a hot plate at 150°C for 30 min to promote solvent evaporation and film stabilization. The presence of the PTFE layer was confirmed by FE-SEM, EDS, and FT-IR analyses. In the SEM images, the PTFE domains appeared as circularly dispersed features on the anodized surface. EDS spectra showed peaks corresponding to C and F, the constituent elements of PTFE. In addition, the PTFE coating was verified by identifying characteristic C–F vibrations in the FT-IR spectra. IR peaks were observed near 1200 cm^{-1} and 600 cm^{-1}, corresponding to CF_2 stretching and C–C/C–F deformation modes, respectively [14] (Fig. 4). Subsequently, laser processing was performed on the surfaces of the PTFE-coated, anodized AA7075 samples. After laser irradiation, the grayish anodized surface became exposed in the regions that had previously been covered with white PTFE. To verify the change in wettability, the contact angle of the laser-treated areas was measured. The contact angle provides information about surface wettability, and hydrophilicity is governed by both surface morphology and surface chemistry. Wan et al. reported that laser exposure of metal surfaces can generate nanofibrous features on the surface [15]. Consistent with this, the laser-treated regions of the PTFE-coated surface exhibited

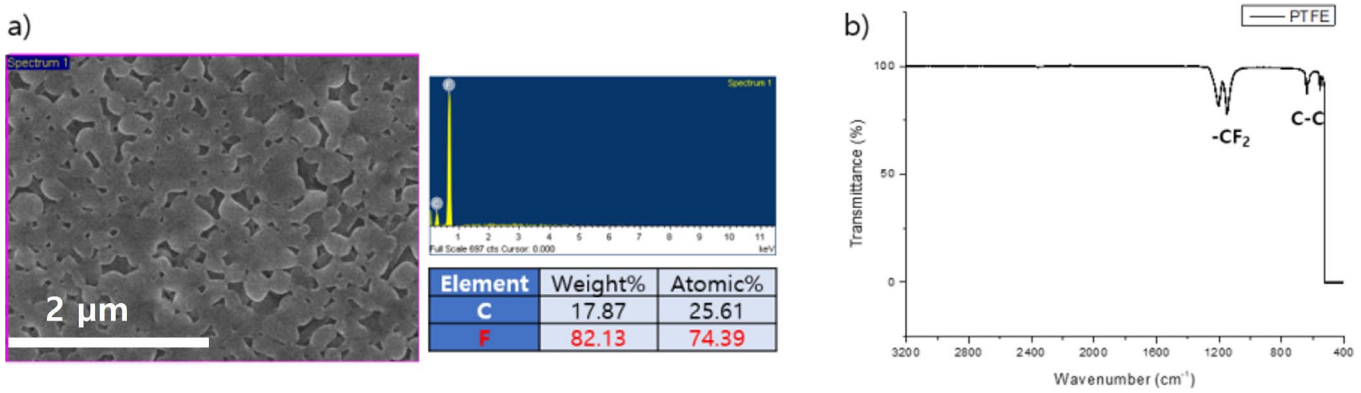

Fig. 4. PTFE confirmation using EDS and FT-IR. a) EDS image of the PTFE-coated surface on anodized AA7075 sample; b) FT-IR results of the PTFE-coated anodized AA7075 sample

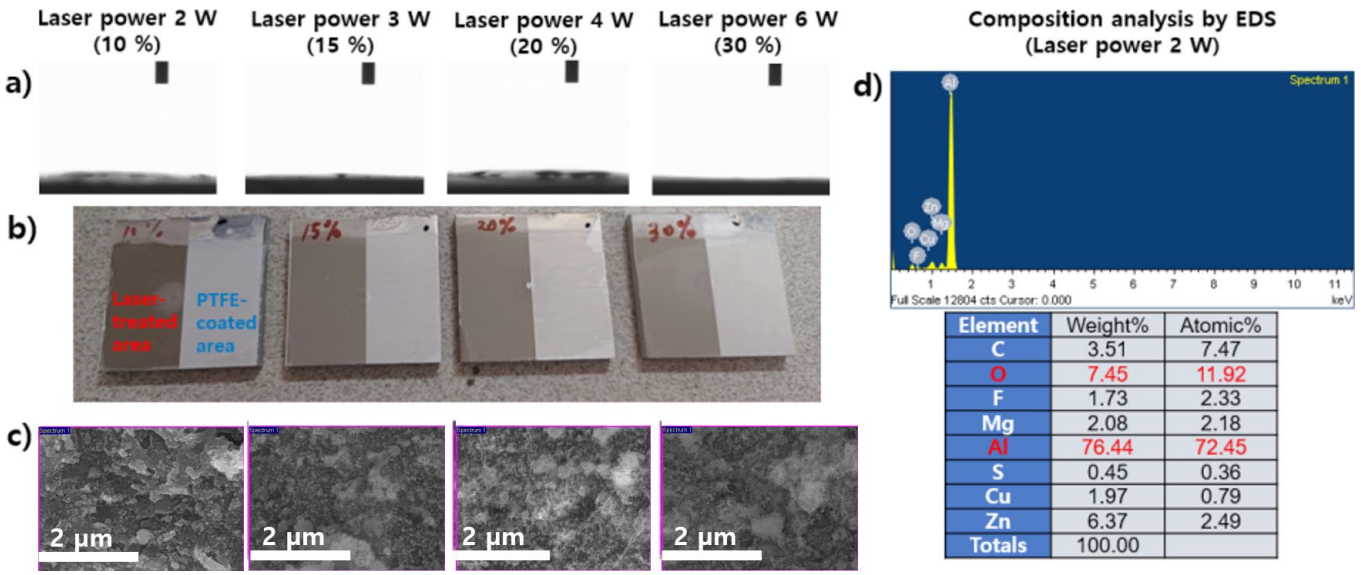

Fig. 5. Contact angle, surface morphology, and EDS analysis results of PTFE-coated, laser-treated anodized AA7075 samples: a) Contact angles of anodized AA7075 samples laser-treated at 2W (10%), 3W (15%), 4W (20%), and 6W (30%) after PTFE coating; b) Anodized AA7075 samples laser-treated at 2W, 3W, 4W, and 6W after PTFE coating; c) FE-SEM images of anodized AA7075 samples laser-treated at 2W, 3W, 4W, and 6W after PTFE coating; d) EDS result of anodized AA7075 samples laser-treated at 2W, 3W, 4W, and 6W after PTFE coating

a thread-like morphology. Hydrophilic surfaces were obtained by irradiating the PTFE-coated areas with a laser power of 2 W (10%). When the laser power was increased to 6 W (30%), the contact angle of the laser-treated surface decreased to nearly 0°, indicating complete wettability (Fig. 5). This behavior may be related to the transformation of the surface morphology into a thread-like structure as the laser power increases. Contact angle images for AA7075 samples with and without PTFE coating and laser treatment are shown in Fig. 6. The average contact angle of the untreated AA7075 surface was 52° (Fig. 6a). After two-step anodizing, however, the surface became hydrophilic regardless of the anodizing voltage (Figs. 6b and 6c). Hydrophilicity, which is associated with surface energy, is largely determined by surface polarity. During anodizing, oxygen-containing bonds form on the surface, markedly reducing the contact angle. In contrast, the PTFE-coated surface exhibited hydrophobicity irrespective of the anodizing voltage (3 or 8 V). When two-step anodizing was conducted at the higher voltage (8 V), smaller and more regularly arranged pores were formed, allowing the PTFE film to pack more densely and thereby increasing the average contact angle from 86° to 111° (Figs. 6d and 6e). The PTFE-coated surface showed low polarity due to the presence of C–F bonds. However, when the surface was irradiated with a 6 W laser, hydrophilicity was restored (Fig. 6f). In the laser-patterned regions, the exposed anodized surface became hydrophilic because the surface polarity increased owing to oxygen bonding [16]. This approach enabled the creation of coexisting hydrophobic and hydrophilic regions on the same anodized AA7075 surface (Fig. 6g).

3.3. Selective Electroless Nickel Plating on Anodized AA7075

Fig. 7 shows the laser setup used for patterning the PTFE-coated AA7075 surface. Grid-shaped laser lines with spacings of 120 µm and 160 µm were successfully fabricated on the PTFE-coated, anodized AA7075. After the PTFE-coated areas were patterned into rectangular or linear features with a width of 200 µm, Ni was deposited by electroless plating. The fundamental mechanism of electroless Ni plating involves the reduction of Ni^{2+} ions to metallic Ni through the oxidation of hypophosphite, during which hydrogen is generated and promotes the reduction reaction [17]. Because the laser-patterned areas were rendered hydrophilic, Ni selectively deposited on these regions. After 5 min of electroless plating, the Ni-deposited areas were clearly distinguishable from the surrounding PTFE-coated regions (Figs. 7b and 7d). However, when the electroless plating time exceeded 10 min, lateral overplating occurred and Ni spread beyond the intended patterned area (Fig. 7c). Therefore, the optimal electroless deposition time was determined to be 5 min. Similar behavior was reported by Jha et al., who observed lateral diffusion of electroless Ni when the immersion time was

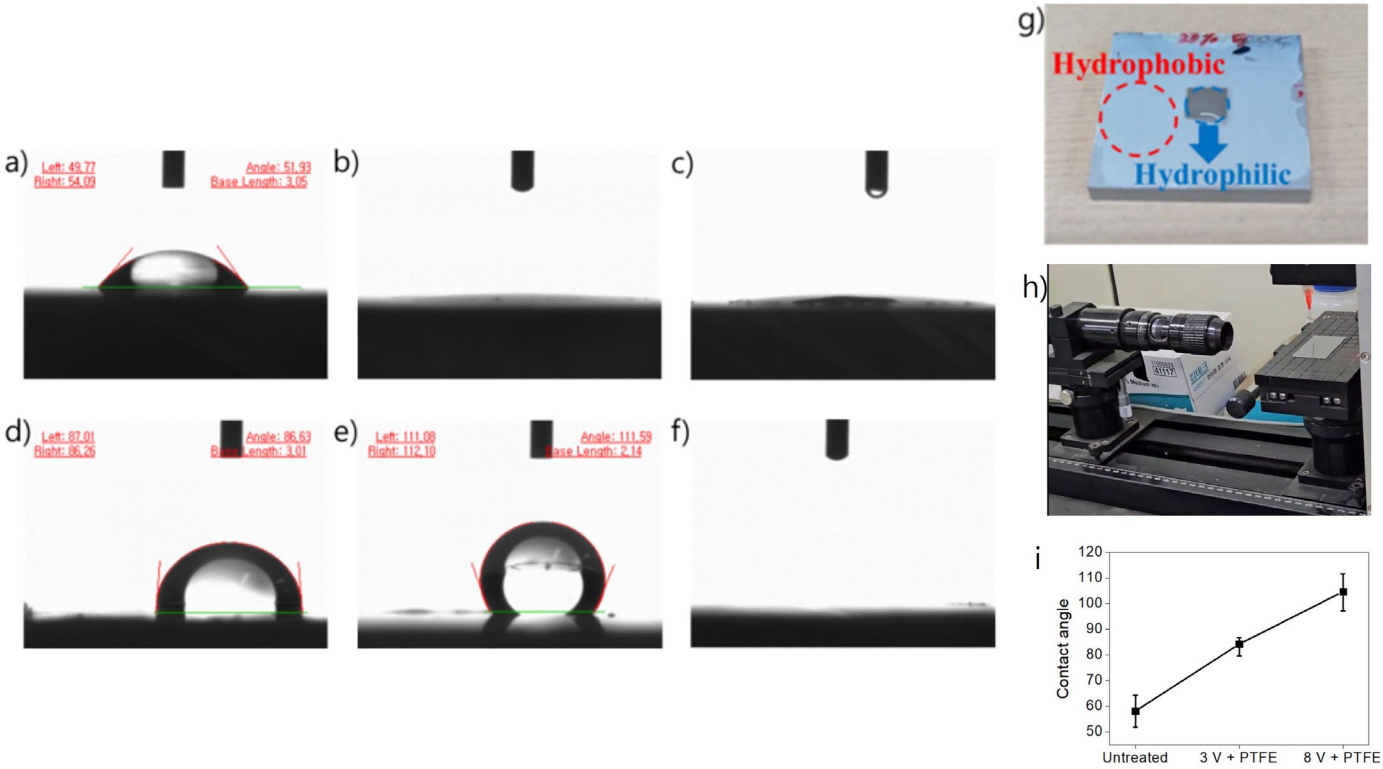

Fig. 6. Contact angle measurement results of a) Untreated AA7075 (no anodization); b) AA7075 sample anodized in two steps at 3 V; c) AA7075 sample anodized in two steps at 8 V; d) AA7075 sample anodized in two steps at 3V and then coated with PTFE; e) AA7075 sample anodized in two steps at 8V and then coated with PTFE; f) AA7075 sample anodized in two steps at 8V, coated with PTFE, and then irradiated with 30% laser power; g) Image of hydrophobic and hydrophilic patterns obtained through laser treatment on PTFE-coated, anodized AA7075; h) Image of contact angle measurement setup; i) Contact angle graph of untreated AA7075, anodized in two steps at 3 V with PTFE coating, and anodized in two steps at 8 V with PTFE coating

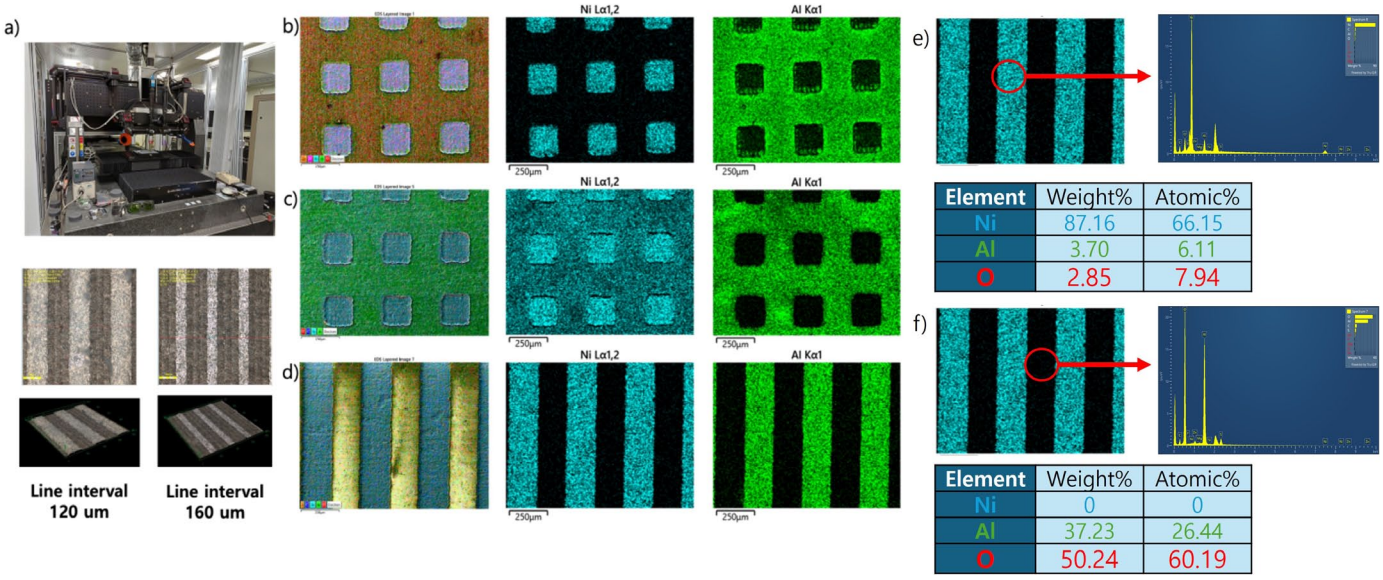

Fig. 7. Setup image for laser patterning and EDS images after electroless nickel plating on laser patterns: a) Laser device setup, and laser pattern on bare AA7075 surface with line interval of 120 μm and 160 μm; b) EDS image after electroless nickel plating for 5 min on laser-patterned hydrophilic area with square interval of 200 um; c) EDS image after electroless nickel plating for 10 min on laser-patterned hydrophilic area with square interval of 200 um; d) EDS image after electroless nickel plating for 5 min on laser-patterned hydrophilic area with line interval of 200 um; e) EDS point analysis of line-patterned area of nickel plated for 5 min; f) EDS point analysis of line-patterned area of PTFE coated in which nickel is non-coated

prolonged [5]. The selective Ni deposition approach presented in this study can be a promising option for industrial applications. By combining laser scanning with PTFE-based surface energy control, the method can be extended to semiconductor packaging and electromagnetic interference (EMI) shielding applications. Moreover, because electroless Ni plating is already an established industrial process, integration of this surface-patterning strategy into existing plating lines should be feasible.

4. Conclusion

In this study, we have demonstrated the direct formation of patterned Ni electrodes on anodized AA7075, a material that can be used as a heat sink. First, a high-density porous anodized surface was achieved through a two-step anodizing process. A hydrophobic surface was then obtained by PTFE spin coating and thermal drying. Anodizing at a higher voltage (8 V), followed by PTFE coating, increased the surface contact angle. Finally, selective Ni deposition was successfully achieved on the anodized AA7075 samples in the laser-activated hydrophilic regions via electroless Ni plating. These results confirm the feasibility of a fully solution-based electrode patterning route that relies on spin coating, laser activation, and electroless deposition, and can be extended to the fabrication of various electrode architectures. In future work, corrosion analyses will be conducted to comprehensively evaluate the corrosion resistance of anodized aluminum films with patterned electrodes. In addition, environmental and durability tests – such as salt spray and temperature cycling – will be performed to assess the long-term stability of the patterned Ni electrodes.

REFERENCES

[1] F. Stippich, E. Vera, H. Scheerer, G.K. Wolf, J-M. Xue, Corrosion properties of alumina coatings on steel and aluminum deposited by ion beam assisted deposition. Surf. Coat. Technol. **98** (1-3), 997-1001 (1998).
DOI: https://doi.org/10.1016/S0257-8972(97)00367-8

[2] H. Shaukatullah, W.R. Storr, B.J. Hansen, M.A. Gaynes, Design and optimization of pin fin heat sinks for low velocity applications. IEEE Trans. Compon. Packag. Manuf. Technol. A **19** (4), 486-494 (1996).
DOI: https://doi.org/10.1109/95.554929

[3] W. Yang, Z. Hu, C. Zhang, Y. Guo, J. Zhao, Screen printing preparation of high-performance flexible planar micro-supercapacitors based on MoS_2 nanoparticles decorated electrochemically exfoliated graphene. Electrochim. Acta **429**, 141041 (2022).
DOI: https://doi.org/10.1016/j.electacta.2022.141041

[4] M. Kim, S.K. Kang, J. Choi, H. Ahn, J. Ji, S.H. Lee, W.B. Kim, Patterning design of electrode to improve the interfacial stability and rate capability for fast rechargeable solid-state lithium-ion batteries. Nano Lett. **22** (24), 10232-10239 (2022).
DOI: https://doi.org/10.1021/acs.nanolett.2c03320

[5] H. Jha, T. Kikuchi, M. Sakairi, H. Takahashi, Area-selective microscale metallization on porous anodic oxide film of aluminium. Electrochem. Commun. **9** (7), 1596-1601 (2007).
DOI: https://doi.org/10.1016/j.elecom.2007.03.003

[6] J. Konieczny, L.A. Dobrzański, K. Labisz, J. Duszczyk, The influence of cast method and anodizing parameters on structure and layer thickness of aluminium alloys. J. Mater. Process. Technol. **157**, 718-723 (2004).
DOI: https://doi.org/10.1016/j.jmatprotec.2004.07.130

[7] A.H. Hamad, Effects of different laser pulse regimes (nanosecond, picosecond and femtosecond) on the ablation of materials for production of nanoparticles in liquid solution. In: High Energy and Short Pulse Lasers, InTech (2016).
DOI: https://doi.org/10.5772/63892

[8] P. Zhang, Y. Zuo, Effects of pore parameters on performance of anodic film on 2024 aluminum alloy. Mater. Chem. Phys. **231**, 9-20 (2019).
DOI: https://doi.org/10.1016/j.matchemphys.2019.04.008

[9] I.C. Chung, C.K. Chung, Y.K. Su, Effect of current density and concentration on microstructure and corrosion behavior of 6061 Al alloy in sulfuric acid. Surf. Coat. Technol. **313**, 299-306 (2017).
DOI: https://doi.org/10.1016/j.surfcoat.2017.01.114

[10] L. González-Rovira, L. González-Souto, P.J. Astola, C. Bravo-Benítez, F.J. Botana, Assessment of the corrosion resistance of self-ordered anodic aluminum oxide (AAO) obtained in tartaric-sulfuric acid. Surf. Coat. Technol. **399**, 126131 (2020).
DOI: https://doi.org/10.1016/j.surfcoat.2020.126131

[11] H. Masuda, M. Satoh, Fabrication of gold nanodot array using anodic porous alumina as an evaporation mask. Jpn. J. Appl. Phys. **35** (1B), L126-L129 (1996).
DOI: https://doi.org/10.1143/jjap.35.L126

[12] G. Patermarakis, K. Moussoutzanis, Transformation of porous structure of anodic alumina films formed during galvanostatic anodising of aluminium. J. Electroanal. Chem. **659** (2), 176-190 (2011). DOI: https://doi.org/10.1016/j.jelechem.2011.05.023

[13] M. Ruan, Y. Zhan, Y. Wu, X. Wang, W. Li, Y. Chen, M. Wei, X. Wang, X. Deng, Preparation of PTFE/PDMS superhydrophobic coating and its anti-icing performance. RSC Adv. **7**, 41339-41344 (2017). DOI: https://doi.org/10.1039/c7ra05264b

[14] D.D. Fazullin, G.V. Mavrin, M.P. Sokolov, I.G. Shaikhiev, Infrared spectroscopic studies of the PTFE and nylon membranes modified polyaniline. Mod. Appl. Sci. **9** (1), 242-249 (2015).
DOI: https://doi.org/10.5539/mas.v9n1p242

[15] H. Wan, S. Li, J. Li, T. Liu, J. Lin, J. Min, Wettability transition of metallic surfaces from laser-generated superhydrophilicity to water-induced superhydrophobicity via a facile and eco-friendly strategy. Mater. Des. **226**, 111691 (2023).
DOI: https://doi.org/10.1016/j.matdes.2023.111691

[16] Y. Tian, L. Jiang, Intrinsically robust hydrophobicity. Nat. Mater. **12** (4), 291-292 (2013). DOI: https://doi.org/10.1038/nmat3610

[17] C.A. Loto, Electroless nickel plating – a review. Silicon **8** (2), 177-186 (2016).
DOI: https://doi.org/10.1007/s12633-015-9367-7